Impact of Chlorine Emissions from Sea-Salt Aerosol on Coastal Urban Ozone

ARTICLE *in* ENVIRONMENTAL SCIENCE AND TECHNOLOGY · FEBRUARY 2003

Impact Factor: 5.33 · DOI: 10.1021/es025793z · Source: PubMed

2 AUTHORS, INCLUDING:

Eladio Knipping
Electric Power Research Institute
69 PUBLICATIONS **1,639** CITATIONS

SEE PROFILE

Environ. Sci. Technol. **2003**, *37,* 275−284

Impact of Chlorine Emissions from Sea-Salt Aerosol on Coastal Urban Ozone

ELADIO M. KNIPPING† AND DONALD DABDUB*

Department of Mechanical and Aerospace Engineering, University of California, Irvine, California 92697-3975

The ability of photochemical models to predict observed coastal chlorine levels and their corresponding effect on ozone formation is explored. Current sea-spray generation functions, a comprehensive gas-phase chlorine chemistry mechanism, and several heterogeneous/multiphase chemical reactions considered key processes leading to reactive chlorine formation are added to an airshed model of the South Coast Air Basin of California. Modeling results reproduce regional sea-salt particle concentrations. The heterogeneous/multiphase chemical reactions do not affect the rate of hydrochloric acid displacement, nor do they enhance aerosol nitrate formation. Chlorine levels in the model are predicted to be an order of magnitude lower than previously observed values at other coastal regions under similar conditions, albeit in much better agreement than previous studies. The results suggest that the inclusion of sea-salt-derived chlorine chemistry might increase morning ozone predictions by as much as 12 ppb in coastal regions and by 4 ppb in the peak domain ozone in the afternoon. The inclusion of anthropogenic sources of chlorine is recommended for future studies, as such sources might elevate ozone predictions even further via direct emission into polluted regions.

1. Introduction

1.1. Background. For over a decade, increasing attention has been focused on the role of chlorine atoms (Cl) as potential oxidants of organic compounds in urban coastal areas (*1*−*4*). However, urban photochemical models have not included reactions to model chlorine chemistry, as significant chlorine-atom concentrations were not believed to develop in these regions (*5*). Indeed, the reaction of hydrochloric acid (HCl) with the hydroxyl radical (OH) to form chlorine atoms is slow, and most of the chlorine present in fresh sea-salt particles, the principal atmospheric chlorine reservoir, is expected to enter the gas phase as hydrochloric acid through displacement by less-volatile and stronger acids (*6*, *7*).

Nonetheless, laboratory studies have shown that sea-salt particles can undergo chemical reactions to form photochemical chlorine-atom precursors (*8*). Field studies confirm the presence of these photolabile chlorine species in coastal regions. Nonspecific measurements of Cl_2*, expected to be primarily molecular chlorine (Cl_2) and some hypochlorous acid (HOCl), up to 254 ppt (≤127 ppt as Cl_2) have been reported in coastal air (*9*). Other investigators have made specific measurements of Cl_2 as high as 150 ppt at a New York coastal site (*10*). In brief, heterogeneous/multiphase chemical reactions on sea-salt particles might enhance daytime chlorine-atom levels beyond those predicted solely due to the gas-phase reaction of hydroxyl radical with hydrochloric acid.

To determine the influence of chlorine chemistry on an urban airshed, this manuscript addresses two important issues: First, can urban photochemical models simulating sea-salt particle formation and chemistry make first-order estimates of observed chlorine levels? Second, how do these chlorine levels affect the formation of ozone in an urban coastal airshed?

1.2. Chlorine Emissions and the Model Domain. The Reactive Chlorine Emissions Inventory (RCEI), a global emissions inventory of reactive chlorine species (defined as those chlorine-containing species with lifetimes of less than 10 years) (*11*−*13*), determined that the majority of chlorine distributed in the troposphere is found within organochlorine compounds. Although important on a global scale, the impact of these species on urban ozone formation, as volatile organic compounds or chlorine-atom precursors, is neglected due to their extended lifetimes and low ambient concentrations.

The majority of inorganic chlorine in the troposphere is found as chloride contained in sea-salt aerosol generated from ocean−wind and ocean−surf interactions (*12*−*14*). There are few other natural sources of inorganic chlorine, with exceptions including particulate chloride contained in wind-blown soils in arid regions and hydrochloric acid emissions from active volcanoes. Anthropogenic sources of inorganic chlorine include coal combustion, biomass burning, and waste incineration. The principal chlorine-containing byproduct of these activities is hydrochloric acid or particulate chloride. Industrial sources contribute to reactive chlorine levels through direct emissions of Cl_2 and HOCl (*15*, *16*).

The terrain of the South Coast Air Basin of California (SoCAB) is characterized by extensive urban development delimited by the forest regions to the north and east and by the Pacific Ocean to the west. The small semiarid region in the northwest section of the domain is unlikely to influence atmospheric chlorine loads significantly compared to the nearby coast. Semiarid regions in the eastern section of the domain are too far downwind to impact the chemistry of the overall basin. Electricity within the basin is generated primarily by oil/gas-fired and hydroelectric power plants (*17*). Given the lack of information on chlorine emissions from sources such as industrial activity and swimming pools, this research shall focus on the determination and quantification of the effect of chlorine originating from the Pacific Ocean on the air quality of the Greater Los Angeles Metropolitan Area.

2. Model Description

2.1. Host Model. The host model used for the current study is based on the California Institute of Technology (Caltech, CIT) Airshed Model (*18*−*23*). In application to the SoCAB, the horizontal domain of the model is an 80 × 30 grid with a resolution of 5 km; vertical resolution consists of five layers up to 1100 m above the surface, sufficient to capture the inversion base of the model domain. The computational domain encompasses the major ocean, surf, urban, and rural regions that influence the air quality of the SoCAB and contains over 90% of the population of the master domain.

* Corresponding author phone: 949-824-6126; fax: 949-824-8585; e-mail:ddabdub@uci.edu; internet: http://albeniz.eng.uci.edu/dabdub.

† Present address: EPRI, 3412 Hillview Ave., Palo Alto, CA 94304.

10.1021/es025793z CCC: $25.00
Published on Web 12/07/2002

The model employs the new Caltech Atmospheric Chemistry Mechanism (CACM), consisting of 361 chemical reactions and 120 fully integrated gas-phase species. CACM includes a detailed treatment of volatile organic compound (VOC) oxidation and has been validated with the August 27−29, 1987, SCAQS episode (*24*).

Dynamic aerosol computations simulate the fate of 37 inorganic and organic aerosol species over 8 size bins, characterized by mass, ranging from 0.039 to 10 μm in diameter. The thermodynamics module Simulating Composition of Atmospheric Particles at Equilibrium 2 (SCAPE2) is used to describe the gas−aerosol partitioning of inorganic aerosol constituents (*25*, *26*). Partitioning of secondary organic oxidation products to either an aqueous or an absorptive organic aerosol phase is determined using a new thermodynamics module coupled to SCAPE2 (*27*). Griffin et al. (*24*) discuss the performance of the CIT Airshed Model in simulating the formation and fate of secondary organic aerosol (SOA) in the SoCAB.

Aerosol particles are modeled using an internally mixed assumption, i.e., all particles within a size bin are assumed to have the same composition. This assumption provides adequate results, particularly in comparisons of measurements of 24-h-averaged concentrations of aerosol constituents with model predictions (*22*).

2.2. Sea-Salt Particle Source Functions. Sea-salt aerosol in the size range pertinent to air-quality studies is produced primarily from the bursting of air-entrained bubbles from oceanic whitecaps formed during the breaking of wind-induced waves (*28*−*37*). Direct production of overly large sea-salt aerosol by spumes is neglected. Open-ocean aerosol fluxes are calculated using the bubble component of the sea-spray function of Monahan et al. (*38*) commonly used in global atmospheric sea-salt aerosol models (*12*, *39*)

$$\frac{dF_{N-Open}}{dr_{80}} = 1.373U_{10}^{3.41}r_{80}^{-3}(1 + 0.057r_{80}^{1.05}) \times 10^{1.19\exp(-B^2)} \quad (1)$$

where $B = (0.380 - \log r_{80})/0.650$. dF_{N-Open}/dr_{80} represents the number of particles generated per unit area of ocean/sea surface per second per unit increment in droplet radius at a reference relative humidity of 80%, r_{80}. U_{10} is the wind speed, in meters per second, at an elevation of 10 meters from the water surface. The corresponding units of eq 1 are particles per square meter per second per micron. This open-ocean source function applies to particles with radii between 0.8 and 10 μm at 80% RH.

Recent investigations report sea-salt aerosol concentrations in the surf zone 1−2 orders higher than the oceanic background (*40*). In this littoral region, wave breaking is dominated by interactions with the sea bottom surface. Extensive, near-complete whitecap coverage can develop even at very low wind speeds. Models of coastal aerosol transport suggest that surf-zone particles and their dispersion into higher levels must be considered in photochemical models including reactions on sea-salt aerosol (*41*). De Leeuw et al. (*40*) developed an expression suitable for the flux of surf-zone aerosol to the coastal boundary layer

$$\frac{dF_{N-Surf}}{dD_0} = 1.1 \times 10^7 e^{0.23U_{10}} D_0^{-1.65} \quad (2)$$

where dF_{N-Surf}/dD_0 represents the number of particles generated per unit area of ocean/sea surface per second per unit increment in droplet diameter at formation, D_0. The units of eq 2 are particles per square meter per second per micron. Equation 2 is applicable for wind speeds up to 9 m/s and for particles with diameters at formation between 1.6 and 20 μm.

Upon ejection, sea-salt particles have a composition similar to that of seawater. SCAPE2 predicts evaporation and condensation rates of water on aerosol particles accounting for relative humidity, temperature, and composition. It is more consistent with the modeling framework to generate particles in their natural form and allow the model to establish their fate. Using the relations (*32*, *34*)

$$\frac{dr_{80}}{dr_0} = 0.506r_0^{-0.024} \quad (3)$$

and

$$\frac{dr_0}{dD_0} = \frac{1}{2} \quad (4)$$

where r_0 is the radius at formation, the open-ocean source function is converted accordingly to

$$\frac{dF_{N-Open}}{dD_0} = \frac{dF_{N-Open}}{dr_{80}} \frac{dr_{80}}{dr_0} \frac{dr_0}{dD_0} \quad (5)$$

The open-ocean and surf-zone source functions incorporated into the airshed model simulate sea-salt aerosol production in a surf-zone span of ∼230 km and an open-ocean region of ∼3850 km^2 within the computational domain. The width of the surf zone was estimated at 100 m, on the higher end of values observed by De Leeuw and co-workers (*40*). However, the model will be unable to capture a portion of particles initially formed beyond the upper diameter limit of the model (10 μm) that will decrease in size to the modeled range when reaching equilibrium with the ambient relative humidity. These compensating effects allow for adequate reproduction of sea-salt aerosol mass.

2.3. Gas-Phase Chlorine Chemistry Mechanism. Twelve gas-phase species and 83 gas-phase reactions have been added to the host model to represent the chemistry of photochemically active chlorine-containing gases derived from sea-salt particles. The rate constants of these reactions reflect the most recent recommendations from IUPAC (*42*, *43*) and NASA/JPL (*44*, *45*) evaluations. These values were corroborated and updated with the latest published results for the oxidation of VOCs by chlorine atoms in the atmosphere (*46*−*51*). The products of isoprene oxidation by Cl atoms were assumed reflecting current knowledge of the mechanism (*52*, *53*).

The gas-phase chlorine chemistry mechanism includes 8 photolysis reactions (Cl_2, HOCl, ClNO, $ClNO_2$, $ClONO_2$, OClO, ClONO, HCOCl), 35 inorganic reactions, the chlorine-atom-initiated oxidation reactions of 14 organic compounds (methane, C_2−C_6 alkanes, C_7−C_{12} alkanes, >C_{12} alkanes, ethene, C_3−C_6 alkenes, >C_6 alkenes, methanol, ethanol, ≥C_2 alcohols, MTBE, C_3−C_6 ketones, >C_6 ketones, isoprene), and 26 intermediate organic reactions

2.4. Heterogeneous/Multiphase Chemical Reactions. The distinction between heterogeneous and multiphase reactions in the field of atmospheric sciences is subtle (*54*). In accordance with common practice, aqueous-phase modeling shall refer to modeling of species solely in an aqueous phase or previously transported from the gas phase, i.e., multiphase modeling. The results of Knipping et al. (*55*) suggest that interfacial reactions confined to gas−liquid interfaces involving gas-phase species, in addition to reactions occurring on solid surfaces, should also be considered as heterogeneous reactions.

In the current study, apart from several equilibrium expressions, aqueous-phase chemical reactions are absent from the computations. Heterogeneous/multiphase chemistry is treated excluding reactions occurring in the bulk

aqueous component of atmospheric aerosol particles. Alternatively, key heterogeneous/multiphase reactions are parametrized to obtain a first-order estimate of chlorine production due to the chemical processing of sea-salt aerosol in urban coastal regions. For the purpose of exploring halogen activation, the composition and water content of urban aerosol might limit aqueous-phase chemistry modeling to the marine-origin component of an external aerosol mixture. (The incorporation of aqueous-phase chemistry into an externally mixed aerosol model is beyond the scope of this study.) Many photochemical models that include aqueous-phase reactions limit the scope of their studies to simulations of the marine boundary layer and clouds (*56*−*60*).

There is strong evidence in support of a mechanism of chlorine formation initiated by the heterogeneous reaction of the hydroxyl radical with chloride ions at the gas−liquid interface of deliquesced salt particles (*55*, *61*).

$$OH_{(gas)} + Cl^-_{(aerosol)} \rightarrow 1/2Cl_{2(gas)} + OH^-_{(aerosol)} \quad (6)$$

Knipping and Dabdub (*62*) determined an overall expression for the rate of reaction 6 using the collision uptake expression

$$R_6 = \frac{1}{2}\frac{d[Cl_2]}{dt} = \gamma_s \frac{\omega}{4} A[OH] \quad (7)$$

where ω is the mean molecular speed of an OH particle and A is the particle surface area. γ_s is the reactive uptake coefficient given by

$$\gamma_s = 0.04[Cl^-] \quad (8)$$

where the constant (0.04) has units of M^{-1}. A dependency on the Cl^- concentration in γ_s is necessary to enhance the reaction as the particles become more concentrated and to quench the reaction as the particles become depleted in chloride. The reader is referred to the original manuscript of Knipping and Dabdub (*62*) for a complete discussion on the methodology, including assumptions and uncertainties, used to reach this expression.

The multiphase reactions of dinitrogen pentoxide (N_2O_5) (*63*−*66*) and chlorine nitrate ($ClONO_2$) (*67*, *68*) with sea-salt particles are also included in the model mechanism

$$N_2O_{5(gas)} + Cl^-_{(aerosol)} \rightarrow ClNO_{2(gas)} + NO_3^-{}_{(aerosol)} \quad (9)$$

$$ClONO_{2(gas)} + Cl^-_{(aerosol)} \rightarrow Cl_{2(gas)} + NO_3^-{}_{(aerosol)} \quad (10)$$

These reactions also release chlorine into the atmosphere in forms that photolyze and generate chlorine atoms. Aqueous-phase models (*56*−*59*) simulate these reactions by transferring the species into sea-salt particles using the mass-transfer method of Schwartz (*69*). The species are assumed to hydrolyze, react with chloride, or react with bromide following a partitioning scheme developed by Behnke and co-workers (*64*, *70*). Stratospheric models use complex phenomenological uptake models not amenable to urban conditions to determine the uptake coefficients of reactions similar to reactions 9 and 10 (*44*, *45*, *71*−*75*).

The method employed by the marine boundary layer models appears promising once a full aqueous-phase and external mixture is incorporated into the model. In the interim, the rates of reactions 9 and 10 were approximated using an expression analogous to eq 7 but with $\gamma_s = 0.02[Cl^-]$. As the model has been modified to investigate only sea-salt interactions, the hydrolysis reactions of N_2O_5 and $ClONO_2$ are not included in the simulations.

The reaction of the nitrate radical, a key nighttime oxidant in urban regions, on sea-salt particles

$$NO_{3(gas)} + Cl^-_{(aerosol)} \rightarrow 1/2Cl_{2(gas)} + NO_3^-{}_{(aerosol)} \quad (11)$$

is added to the other reactions in a sensitivity simulation to gain insight into the effect of a potential nocturnal mechanism for chlorine release from sea-salt particles. The possibility of this reaction occurring, and the extent to which it might occur, is uncertain. This reaction is modeled in a fashion similar to reactions 9 and 10.

Included in the SCAPE2 thermodynamic module (*25*, *26*) of the CIT Airshed Model are several heterogeneous/multiphase equilibrium expressions that account for HCl displacement by less-volatile and stronger acids, such as nitric and sulfuric acids. These reactions can be summarized as follows

$$HNO_{3(gas)} + XCl_{(aerosol)} \rightleftharpoons HCl_{(gas)} + XNO_{3(aerosol)} \quad (12)$$

$$H_2SO_{4(gas)} + 2XCl_{(aerosol)} \rightleftharpoons 2HCl_{(gas)} + X_2SO_{4(aerosol)} \quad (13)$$

$$H_2SO_{4(gas)} + XCl_{(aerosol)} \rightleftharpoons HCl_{(gas)} + XHSO_{4(aerosol)} \quad (14)$$

where X denotes a cation such as Na^+, NH_4^+, K^+, or H^+. Other equilibrium reactions are included in the SCAPE2 module that form diprotic salts (involving Mg^{2+} and Ca^{2+}), in addition to further reactions that form carbonate and bicarbonate salts.

The reaction of hydrochloric acid with the hydroxyl radical in the gas phase

$$HCl + OH \rightarrow Cl + H_2O \quad (15)$$

is relatively slow. Therefore, although most of the chloride is expected to exit the sea-salt particles as HCl by reactions 12−14, it is reactions 6 and 9−11 that are expected to enhance chlorine radical concentrations in the model because of their highly photolyzable gaseous products.

2.5. Meteorology and Emissions. Air-quality simulations of conditions from September 8, 1993, (0000 PST) to September 9, 1993, (2400 PST) are performed in this study. September 8, 1993, is used as a model spin-up day to decrease the importance of model artifacts (initial conditions, boundary conditions) in the predictions of results presented for September 9, 1993.

During the episode, conditions were sunny and hot, with peak temperatures in the eastern region of the domain exceeding 40 °C, leading to enhanced photooxidation rates. Typical wind speeds during the scenario ranged from 1 to 3 m s^{-1}, with higher wind speeds experienced during early afternoon. Typical relative humidity near the surf zone ranged from 70 to 90%, with a higher relative humidity present during milder nocturnal hours. Meteorological data for this episode were supplied from hourly observations gathered by the South Coast Air Quality Management District (SCAQMD) (*23*). The derivation of hourly gridded meteorological fields for relative humidity, temperature, ultraviolet radiation, and total solar radiation follows the method described by Harley et al. (*20*). Fraser et al. (*76*) describe the methodologies used to generate hourly three-dimensional wind fields and hourly mixing-depth fields that accurately represent the base height of the temperature inversion prevailing over the Los Angeles area.

Hourly gridded gas and particulate emissions inventories for this episode were supplied directly by the South Coast Air Quality Management District (*23*), except for sea-salt particle emissions, which were calculated using either the open-ocean or surf-zone sea-salt particle source functions described earlier. Hourly aerosol emissions are apportioned

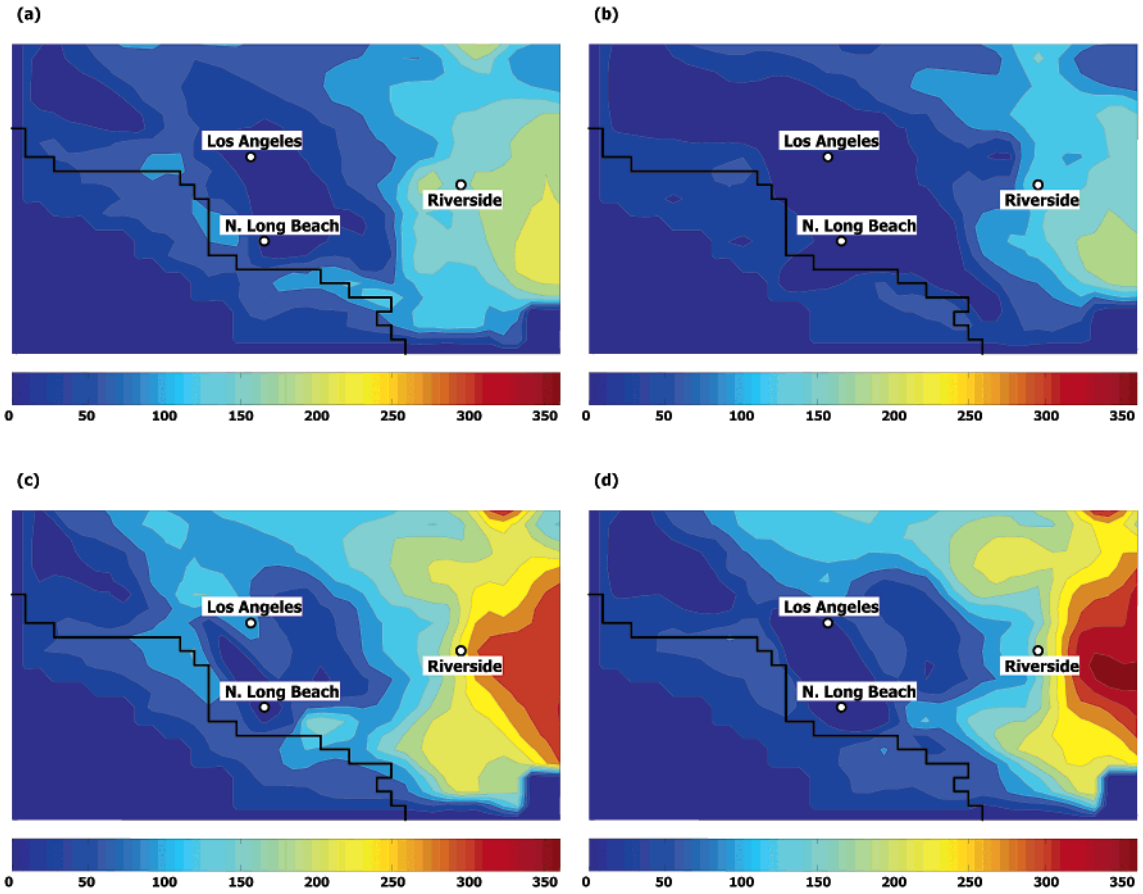

FIGURE 1. Ground-level ozone mixing-ratio contours for September 9, 1993 (all values in parts per billion). Shown are diagrams illustrating the mixing ratio value predicted by the base-case simulation at (a) 1000, (b) 1200, (c) 1500, and (d) 1800 PST.

into eight size sections, and the appropriate mass of each species is placed into the proper size bin of the corresponding cell (*76*).

3. Simulations and Results

3.1. Base-Case Simulation. A base-case simulation was performed to evaluate the effect of sea-salt-derived chlorine chemistry. The results of this simulation provide a benchmark of ozone predictions without the effect of the added chemical reactions, i.e., the complete gas-phase chlorine chemistry mechanism and four of the heterogeneous/multiphase reactions (*6*, *9*−*11*). Equilibrium reactions (*12*−*14*) treated by the SCAPE2 thermodynamic module were included in these simulations to account for chloride depletion due to HCl displacement by less-volatile stronger acids. The newly incorporated sea-salt particle source functions were also included in the base-case simulation.

Griffin et al. have evaluated the adequacy of the CIT Airshed Model in representing O_3, NO_x, and VOC levels for the September 8−9, 1993, episode (*23*), essentially reproducing the base-case simulation. The authors concluded the evolution of these species is predicted with accuracy consistent with that of previous simulations of the SCAQS episode (*24*) used to validate the CACM chemical mechanism. Nonetheless, Figure 1 manifests the complexity of the air-quality episode selected for this study. Ozone contour plots illustrate the characteristic increase of ozone throughout the eastern region of the domain as the day progresses. Low ozone mixing ratios in the center region of the domain are attributed to NO_x titration of ozone by the model. Investigations of the conversion of nitric acid into photochemically active NO_x suggest that the inclusion of "renoxification" might provide a means for reconciling modeled ozone predictions with observations in this region (*77*).

The eastern boundary of the domain retains elevated nighttime ozone mixing ratios for two reasons. First, numerical models encounter inherent difficulties when simulating meteorological conditions at the mountainous boundary of the computational domain. Second, Griffin et al. (*23*) have determined that the conventional method used to calculate vertical eddy diffusivities in the CIT Airshed Model underpredicts these parameters at the low wind speeds characteristic of this episode. Indeed, unusually high simulated nighttime concentrations of tracer pollutant and secondary species are predicted in a large region of the domain. The underestimation of vertical mixing is attributed to a lack of consideration of urban heat islands and mechanical mixing near roadways during the calculation of diffusion parameters.

The air-quality episode presents several interesting challenges to the air-quality modeling community. However, the model is reasonably well-behaved. Ozone mixing ratios in monitoring stations reached values near 300 ppb during the episode (*78*), as predicted by the model. Furthermore, the overall model response is adequate for the purposes of the current study, i.e., comparison of the base-case model results to simulations including chlorine chemistry.

3.2. Sea-Salt Particles Loads. This section presents characteristics of the sea-salt particle loadings in the South Coast Air Basin of California as predicted by the CIT Airshed Model and evaluates the performance of the sea-salt aerosol source functions. Values are presented for the "Case Cl Chem" simulation, a scenario similar to the base-case simulation, now incorporating the complete gas-phase chlorine chem-

TABLE 1. Comparison of Observed and Predicted Ground-Level 24-h-Average Particulate Sodium Concentrations for September 9, 1993[a]

	Long Beach		Claremont	
	$PM_{2.5}$ sodium	TSP sodium	$PM_{2.5}$ sodium	TSP sodium
observed	0.50	3.11	0.64	1.09
	$PM_{2.5}$ sodium	PM_{10} sodium	$PM_{2.5}$ sodium	PM_{10} sodium
modeled	0.91	2.65	0.28	0.62

[a] All values in $\mu g/m^3$.

istry mechanism and three heterogeneous/multiphase reactions (reactions 6, 10, and 11).

Sea-salt and aerosol chloride concentrations are dominated by the surf-zone production of sea-spray; the open-ocean contribution to coastal aerosol concentrations is negligible. Higher sea-salt aerosol concentrations are generated in coastal regions that are oriented in line with the general westerly wind patterns of the air basin as surf-zone-generated aerosol accumulates in these regions. Although some sea-salt particles do travel for several tens of kilometers inland, concentrations are low. Most of the sea-salt aerosol mass produced in coastal regions is generated as larger particles that deposit fairly quickly. Table 1 compares observed versus modeled 24-h-average ground-level particulate sodium concentrations at locations in Long Beach and Claremont, approximately 10 km north and 50 km northeast of the nearest coast. (Modeled values of particulate sodium and chloride originate wholly from sea-salt aerosol. Although it is not possible to adjust the measured values of sodium to reflect only sea-salt sodium, it is reasonable to infer that, in a coastal region, the majority of the sodium measured is from the oceanic source.) During the observation, total suspended particulate matter (TSP) concentrations were measured instead of actual PM_{10} concentrations. However, because of gravitational settling of very large particles, most of the sodium mass should be within the modeled bins (diameters $\leq 10\ \mu m$) at fetches this far from the coast. The results from the comparison suggest that sea-salt particles are modeled well by the CIT Airshed Model and the newly integrated sea-salt particles source functions. The underestimation of vertical mixing mentioned earlier is a possible explanation of the prediction of sodium concentrations lower than observed values at the Claremont site. Near the coast, vertical mixing disperses aerosol mass to higher layers and can lead to the dilution of aerosol mass. However, efficient vertical mixing can enhance downwind concentrations by reducing the likelihood of deposition in lower layers during transport, thus allowing for dispersion afterward in the downwind location of particulate sodium in the upper layers to the lower layer.

Remote marine boundary-layer aerosol populations have been observed to consist of approximately 100−300 particles cm^{-3}, with 5−30 particles cm^{-3} being directly emitted sea-salt particles (*79*). Modeled 24-h-averaged oceanic aerosol size distributions approximately 15 km from the coast are consistent with the character of a marine aerosol population influenced by a relatively nearby urban region. Low sea-salt concentrations are indicative of the low wind speeds of the episode. The larger size bins consist mostly of marine aerosol constituents, non-sea-salt (nss) sulfate, nitrate, organics and unclassified material (e.g., dust). The smaller size bins are dominated by nss sulfate, organics, and unclassified material.

In model predicted 24-h-averaged coastal aerosol size distributions, both the urban and marine components of the distribution are increased compared to the more distant oceanic distribution. The concentrations of the marine

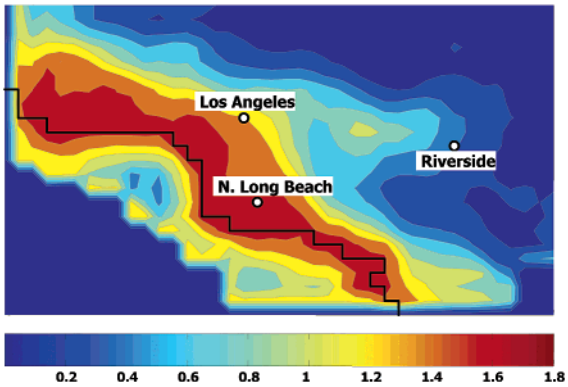

FIGURE 2. Model-predicted 24-h-average aerosol mass ratios of PM_{10} chloride to PM_{10} sodium for September 29, 1993. Shown are results for the lowest model layer, i.e., ground level, extending up to 38.5 m. Only oceanic sources of sodium and chloride are included in the analysis. (Fresh sea-salt particle ratio $\approx$ 1.8.)

aerosol constituents in the larger bins are greatly enhanced as a result of the surf-zone functions developed by De Leeuw and co-workers (*40*) for conditions off the California coast. These values are consistent with this group's observation of enhancement of sea-salt particle concentrations by 1−2 orders of magnitude over the surf region.

A freshly ejected sea-salt particle is expected to have a mass concentration ratio of chloride to sodium of ~1.8. This ratio is predicted in the region of strongest sea-salt aerosol production, the surf zone. Chloride-to-sodium ratios calculated throughout the basin, shown in Figure 2, illustrate chloride depletion, predicted by the model as a result of hydrochloric acid displacement, as marine aerosol particles travel away from their surf-zone source. In the SoCAB, displacement occurs primarily by nitric acid. The newly added heterogeneous/multiphase chemical reactions do not significantly affect the rate of acid displacement, nor do they enhance aerosol nitrate formation. (Although the main fate of reactive chlorine is the formation of HCl, the majority of HCl still originates from acid displacement.) These results for an episode in early September 1993, are in qualitative agreement with observations of chloride deficits, attributed to displacement by nitric acid, made for another episode in late September 1996 (*6*, *7*). Chloride depletion is also predicted in the open because of the transport of pollutants from the continent (and previously depleted particles) due to sea-breeze/land-breeze cycles and maritime vessel emissions.

3.3. Model Results: Cl_2 Levels and Impact of Chlorine Chemistry on Ozone Formation. Observations of chlorine levels in the South Coast Air Basin of California have not been reported. However, the analogous conditions of previously reported Cl_2 measurements (*9*, *10*)—on-shore winds toward coastal regions—allow for comparison with these model results. As shown in Figure 3, the high chlorine mixing ratios measured by other investigators cannot be reproduced by the model. The maximum ground level 1-h-average Cl_2 concentration predicted by the Case Cl Chem simulation is 12 ppt, predicted both in the late evening and at predawn. Although the model predicts mixing ratios an order of magnitude below observed values, these values represent an increase by a factor of 30 in the ability to reproduce Cl_2 mixing ratios when compared to the maximum Cl_2 levels predicted by the box model of Spicer et al. (*10*).

Although the Cl_2 levels predicted here are below observed values, an analysis of the influence of the sea-salt-derived chlorine chemistry in this simulation on ozone formation dynamics is performed by determining the difference between the mixing ratios predicted in the Case Cl Chem simulation and the mixing ratios predicted in the base-case

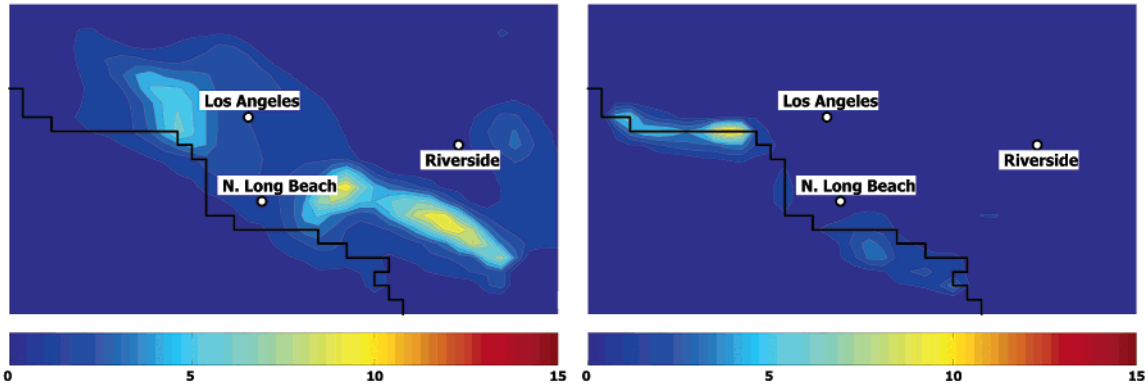

FIGURE 3. Ground-level chlorine (Cl_2) mixing ratio contours for September 9, 1993 (all values in parts per billion). Shown are diagrams illustrating the mixing ratio value predicted by the Case CI Chem simulation at (left) 2200 and (right) 0800 PST.

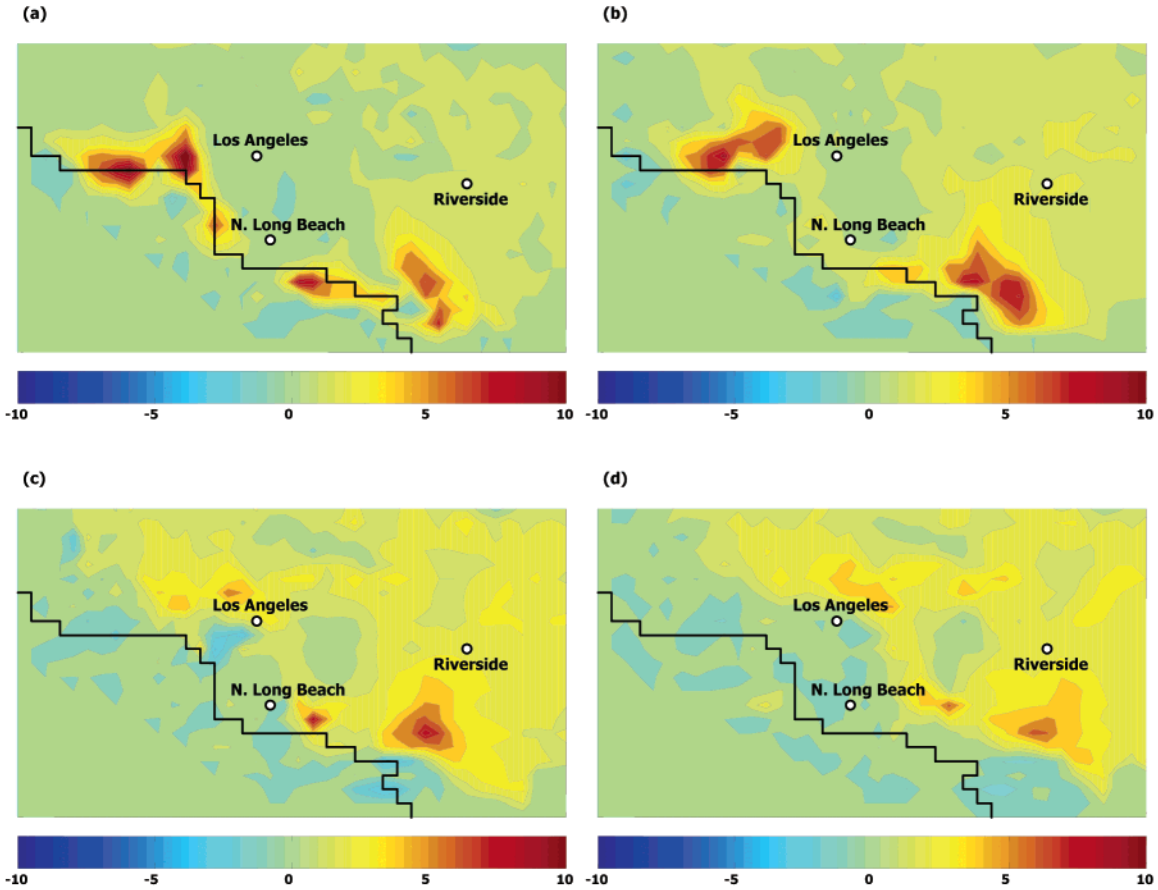

FIGURE 4. Ground-level ozone mixing ratio difference contours for September 9, 1993 (all values in parts per billion). Shown are diagrams illustrating the value obtained by subtracting the ozone mixing ratios predicted by the Case CI Chem simulation from the ozone mixing ratios predicted by the base-case simulation at (a) 1000, (b) 1200, (c) 1500, and (d) 1800 PST.

simulation. Figure 4 shows that sea-salt chemistry, even when Cl_2 levels are underpredicted, can contribute to ~10 ppb in ozone mixing ratios in certain regions. These ozone differences between the simulations are at a maximum in the morning. Although the influence dissipates in later hours, the fraction of the basin affected by the chlorine chemistry increases through the influence of various physicochemical processes, predominantly transport.

Ground-level ozone predictions for 36 individual monitoring stations found in distinct grid cells within the South Coast Air Basin of California are analyzed. The peak ozone mixing ratio at all stations increases by an average of 2.3 ppb, with some stations increasing their peak O_3 by 4 ppb. The stationwide peak ozone increases by 2.2 ppb, and the domain peak O_3 concentration increases by 3.9 ppb. However, ozone mixing ratios increase by greater amounts at times that do not coincide with the peak ozone mixing ratios. The highest 1-h increase in ozone is predicted at 7.7 ppb at a station in the middle of the domain. The highest increase in ozone in the domain at any grid cell at any hour is predicted to reach 12.7 ppb. If the analysis is limited only to cells exceeding the California 1-h ozone standard of 90 ppb, the highest 1-h ozone increase is calculated at 11.7 ppb.

3.4. Surrogate Nighttime Reaction. The field-measurement and model analysis of Spicer and co-workers (*10*) suggested the existence of an unexplained nighttime source of molecular chlorine in coastal regions that allowed for nocturnal accumulation of chlorine up to predawn hours. A surrogate reaction of sea-salt particles with the nitrate radical, similar to that with the hydroxyl radical, is included in the

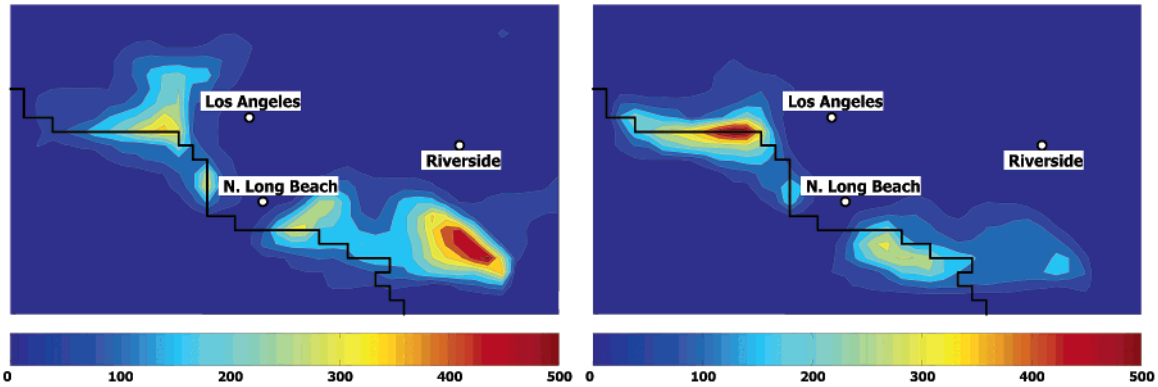

FIGURE 5. Ground-level chlorine (Cl_2) mixing ratio contours for September 9, 1993 (all values in parts per billion). Shown are diagrams illustrating the mixing ratio value predicted by the Case Cl Chem + NO_3 Reaction simulation at (left) 2200and (right) 0700 PST.

TABLE 2. Summary of Simulation Scenarios

simulation name	description
base case	simulation *without* gas-phase chlorine chemistry or heterogeneous/multiphase chemistry on sea-salt particles, except for acid displacement reactions; used as benchmark for other simulations
Case Cl Chem	simulation *including* heterogeneous/multiphase reactions of OH, N_2O_5, and $ClONO_2$ on sea-salt particles and full mechanism of gas-phase chlorine chemistry
Case Cl Chem + NO_3 Reaction	same as Case Cl Chem with a surrogate nighttime reaction of the nitrate radical on sea-salt particles; simulation evaluates the impact of a potential nighttime mechanism for chlorine generation
$[Cl_2] = 150$ ppt	same as Case Cl Chem but prescribing a constant Cl_2 mixing ratio of 150 ppt throughout the model domain; simulation provides insight into effect of increased chlorine levels in the region
$[Cl_2] = 1500$ ppt	same as above but prescribing a constant Cl_2 mixing ratio of 1500 ppt; simulation used to test how high Cl_2 mixing ratios need to be to affect temporal and spatial dynamics of ozone formation

model (reaction 11). There is evidence of a similar reaction of the nitrate radical on dilute NaCl solutions and dry NaCl (*80*−*82*), leading to formation of chlorine atoms. (The nature of the true nighttime chemistry leading to Cl_2 formation is uncertain, with some researchers suggesting a ferric-ion-catalyzed reaction of chloride with background ozone (*83*) in lieu of a nitrate-radical-initiated mechanism.) Notwithstanding the uncertainties, this modeling scenario, denoted as "Case Cl Chem + NO_3 Reaction", provides a sensitivity analysis of the impact of a nighttime mechanism for Cl_2 accumulation.

The incorporation of this reaction increases the prediction of Cl_2 to values more consistent with the measurements of Spicer et al. (*10*) and Keene et al. (*9*), as shown in Figure 5. In a few areas, the predicted values actually exceed those measured by the field campaigns by up to a factor of 4, but good agreement is obtained in general. The increase in Cl_2 does not endure past the dawn, when photolysis of both NO_3 and Cl_2 brings the molecular chlorine concentration down to levels similar to those found in the Case Cl Chem simulation. Consequently, the impact on ozone mixing ratios of adding the nitrate radical reaction on the sea-salt particles is not as marked as the impact on predawn Cl_2 levels. Morning differences between ozone predictions in this scenario versus the base case are increased by <2 ppb in coastal regions when compared to those illustrated in Figure 3 for the Case Cl Chem simulation, with the effect lessening throughout the day. Overall, similar ozone formation dynamics are exhibited by the Case Cl Chem + NO_3 Reaction simulation and the Case Cl Chem simulation.

3.5. Additional Sensitivity Simulations. The preceding simulations lack the contribution of anthropogenic sources of chlorine. Studies in Texas indicate that the contribution of anthropogenic sources of chlorine might also be of concern (*84*, *85*). Potential anthropogenic sources of Cl_2 and HOCl include direct emission from industrial activities, emission from the use of biocides in cooling towers, emission from water and wastewater treatment, and emission from swimming pool treatment. These sources can raise photochemically active chlorine levels not only near the coast but throughout the model domain.

In view of these studies, two sensitivity simulations were performed to estimate the impact of an increased burden of reactive chlorine on smog formation in the South Coast Air Basin of California: a simulation prescribing a constant Cl_2 mixing ratio of 150 ppt in all grid cells on all levels, denoted as "$[Cl_2] = 150$ ppt", and a simulation where the constant Cl_2 mixing ratio is prescribed at an extreme (and unrealistic) value of 1500 ppt in all levels, designated "$[Cl_2] = 1500$ ppt". Specifically, these simulation suggest the levels at which chlorine must be present to affect the temporal and spatial dynamics (in addition to the magnitude) of ozone formation.

In the case where chlorine mixing ratios are held constant at 150 ppt the effect is primarily an overall increase in ozone levels in the range of 30−100 ppb (or 15−110%) depending on location. However, no change in the temporal and spatial dynamics of ozone formation is exhibited. A discrete enhancement of ozone formation during early hours can only be achieved by prescribing an extreme chlorine mixing ratio of 1500 ppt, with two distinct (and highly exaggerated) ozone peaks forming near central Los Angeles and Riverside.

4. Discussion

A descriptive summary of all model simulations is provided in Table 2. A quantitative measure of the impact of chlorine chemistry on ozone as exhibited in all scenarios is presented in Table 3. Included are values from the analysis of 36 monitoring stations found in distinct grid cells within the air basin.

In brief, the addition of chlorine chemistry in the Case Cl Chem scenario increases the ozone mixing ratios near the coast shortly after sunrise. The effect dissipates as the day continues, but physicochemical processes simulated in the model, primarily transport and increased oxidation rates due to enhanced ozone levels, transmit the influence throughout

TABLE 3. Summary of Ozone Metrics as Predicted by the Simulations[a,b]

region	base case	case 1	case 2	case 3	case 4
		peak [O_3]			
stationwide	353.3	355.5	355.6	406.6	591.6
domain	406.2	410.1	410.0	468.9	601.3
		Δ peak 1-h [O_3]			
stationwide[c]		2.2	2.3	53.3	238.3
domain		3.9	3.8	62.7	195.1
		max Δ 1-h [O_3]			
stationwide[c]		7.7	7.4	136.3	532.1
domain		12.7	13.7	139.2	538.1
domain over 80 ppb		12.5	11.5	139.2	538.1
domain over 90 ppb		11.7	9.6	139.2	538.1

[a] All values correspond to ground-level model predictions for September 9, 1993, and are in units of parts per billion. [b] Case numbers: 1, Case Cl Chem; 2, Case Cl Chem + NO_3 Reaction; 3, Case [Cl_2] = 150 ppt; 4, Case [Cl_2] = 1500 ppt. [c] Change in 1-h peak stationwide O_3 mixing ratio (not necessarily same location) and maximum of 1-h change in O_3 mixing ratio at any station at any time.

the region. The destruction of O_3 by Cl atoms is not significant in urban regions compared to enhancement of VOC−NO_x cycle. As illustrated in Figure 4, only in a few small patches of the domain with low pollutant concentrations, primarily in the open ocean and in the southern coast of the domain, are ozone predictions decreased slightly.

The ozone increases observed might be mathematically subtle in relation to the total mixing ratios in areas where ozone levels are high. However, it is evident that the addition of chlorine chemistry serves primarily to increase the total ozone exposure of the population. In addition, considering that background O_3 levels hover around 40 ppb and that standards are set at 80 ppb, an increase of 10 ppb is equivalent to removing a quarter "slack" available between background ozone and an air-quality standard violation.

The parametrizations used to release reactive chlorine in the Case Cl Chem might oversimplify (and even overestimate) the reactions of hydroxyl radical, dinitrogen pentoxide, and chlorine nitrate on sea-salt particles. Nonetheless, the simulation fails to predict Cl_2 mixing ratios when compared to observed values. Two explanations are apparent: (1) other sources govern chlorine concentrations in coastal urban regions, or (2) other unknown reactions on/within sea-salt particles are more efficient in releasing chlorine. Since the observations of Keene et al. and Spicer et al. (*9*, *10*) were made on air parcels traveling toward the coast, it appears more probable that the current underprediction is a result of an unknown (probably nighttime) mechanism of chlorine release. Indeed, the reaction of the nitrate radical with sea-salt particles is included in an additional simulation as a surrogate for precisely this kind of unknown mechanism of chlorine production. The Case Cl Chem + NO_3 Reaction predicts much higher predawn Cl_2 levels than the Case Cl Chem simulation, with mixing ratios reaching up to 600 ppt. However, the effect on ozone mixing ratios predicted by the model is not as marked. Although urban sources of chlorine might also affect the magnitude of chlorine concentrations, it is more likely that these sources govern reactive chlorine concentrations inland and not at the coast.

These results do present an interesting query: Why do ozone levels remain fairly unaffected in the Case Cl Chem + NO_3 Reaction simulation when compared to the Case Cl Chem simulation? A rigorous answer to this question can only be obtained through sensitivity analysis of the chemical mechanism with respect to the modeling episode in question. However, an analysis of the relative concentrations of OH and Cl radicals in each simulation yields insightful results.

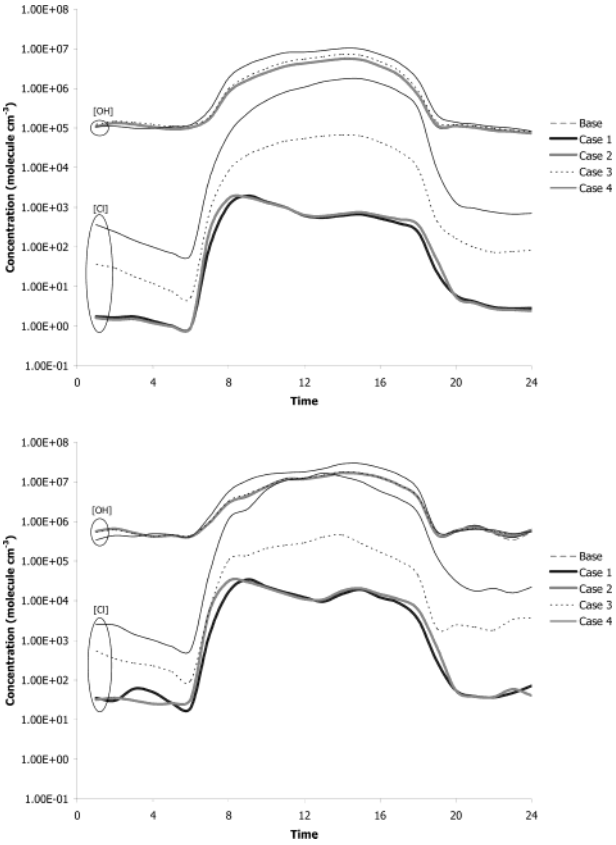

FIGURE 6. Model-predicted OH and Cl concentration time series: (top) ground-level domain-averaged 1-h-average concentrations and (bottom) ground-level maximum individual-cell 1-h-average concentrations (values do not necessarily correspond to same cell) for September 9, 1993. Case Numbers: 1, Case Cl Chem; 2, Case Cl Chem + NO_3 Reaction; 3, Case [Cl_2] = 150 ppt; 4, Case [Cl_2] = 1500 ppt.

The principal mechanism leading to ozone formation is well-recognized (*79*, *86*, *87*). Briefly, OH radicals initiate the oxidation of organic compounds leading to the formation of organic peroxy (RO_2) and hydroperoxy (HO_2) radicals. RO_2 and HO_2 radicals oxidize nitric oxide (NO) to nitrogen dioxide (NO_2). Nitrogen dioxide then photolyzes to form ground-state oxygen atom, $O(^3P)$, which undergoes an association reaction with oxygen to form ozone. The chlorine-atom-initiated oxidation of organics needs to occur at rates similar to that of the OH-initiated oxidation to influence this mechanism. The rate constants for the reactions of Cl radicals with most organic compounds are 1−2 orders of magnitude higher than the corresponding rate constants for reactions with OH, with many reactions occurring at the collision-controlled rate. Thus, Cl atom concentrations need to be present within ~2 orders of magnitude of OH concentrations to play a role in ozone chemistry.

Figure 6 exhibits times series for domain-averaged 1-h ground-level hydroxyl and chlorine radical predictions. Time series showing values of the individual cell containing the maximum values are also shown. The peak OH levels are predicted around 2:00 p.m. for all simulations, whereas peak Cl concentrations are predicted at 8:00 and 9:00 a.m. for the Case Cl Chem + NO_3 Reaction and the Case Cl Chem scenarios, respectively. It is only during morning hours that Cl atoms compete favorably with the OH radical, when coastal concentrations are within a factor of ~130−140 of maximum OH concentrations and a factor of ~25−30 of the domain-averaged OH concentration. Chlorine atoms might dominate the oxidation of some organic compounds in this region. However, this predominance is limited to the coast as the

domain-averaged concentration of Cl is ~700−800 times lower than domain-averaged concentration of OH.

Chlorine-radical-initiated oxidation of organics cannot compete as favorably with OH-initiated oxidation during the remainder of the morning and throughout the afternoon. Coastal Cl concentrations during this period are typically 750−800 times below maximum OH concentrations and 180−190 times below the domain-averaged OH concentration. Furthermore, domain-averaged Cl concentration is over 5000 times less than domain-averaged OH concentration. Overall, there is little difference in the evolution of the chlorine-atom concentration between the Case Cl Chem and the Case Cl Chem + NO_3 Reaction simulations, except for a shift in the timing of the peak concentration.

In summary, the results of these simulations suggest that the inclusion of sea-salt-derived chlorine chemistry in photochemical models might increase morning ozone predictions by as much as ~12 ppb in coastal regions and by ~4 ppb in the peak domain ozone in the afternoon. The peak ozone mixing ratios at most monitoring sites increases by 2−4 ppb, and even higher ozone increases, up to 7 ppb, are predicted at other times not coinciding with the peak. Overall, ozone exposure is increased throughout the domain.

Researchers have estimated and collected chlorine emissions data from various anthropogenic and natural sources in the Houston Metropolitan Area (*85*). The discharge of reactive chlorine in the region was approximated to emanate chiefly from cooling towers (47%), swimming pools (39%), and industry (11%). Sea-salt particles were assumed to contribute to only 3% of chlorine emissions, although the authors recognize that their approximation of sea-salt-derived emissions is highly uncertain. Evaluations of the contribution of chlorine chemistry to enhanced ozone predictions yield results strikingly similar to those of the present study, which does not include anthropogenic sources of chlorine. For various late-summer simulation scenarios, morning ozone predictions are increased by 11−16 ppb. Afternoon maximum ozone enhancements are in the range of 5−7 ppb (not necessarily coinciding with the location of the peak).

Anthropogenic sources in the South Coast Air Basin of California might contribute significantly to chlorine loads in the atmosphere. Depending on their spatial distribution, these sources might provide a greater opportunity to enhance ozone formation by emitting chlorine gases directly into regions rich in hydrocarbons and oxides of nitrogen. The combined effects of oceanic and urban chlorine sources in the South Coast Air Basin warrant further investigation. Future sensitivity analysis should also evaluate the effect of chlorine chemistry in VOC-limited regimes versus NO_x-limited regimes, as well as the evolution of reactive chlorine gases in air masses originating from coastal urban regions that are transported primarily over the ocean.

Acknowledgments

The authors are grateful to the National Science Foundation for financial support under CAREER Grant ATM-9985025 and the California Air Resources Board under ARB Contract 00-324. The statements and conclusions in this manuscript do not necessarily reflect the views of the National Science Foundation or the California Air Resources Board. E.M.K. thanks the Link Foundation for fellowship support.

Supporting Information Available

Gas-phase chlorine chemistry mechanism extensions to the Caltech Atmospheric Chemistry Mechanism (CACM) and additional tables and figures illustrating model results. This material is available free of charge via the Internet at http://pubs.acs.org.

Literature Cited

(1) Keene, W. C.; Pszenny, A. A. P.; Jacob, D. J.; Duce, R. A.; Galloway, J. N.; Schultz-Tokos, J. J.; Sievering, H.; Boatman, J. F. *Global Biogeochem. Cycles* **1990**, *4*, 407.
(2) Finlayson-Pitts, B. J. *Res. Chem. Intermed.* **1993**, *19*, 235.
(3) Pszenny, A. A. P.; Keene, W. C.; Jacob, D. J.; Fan, S.; Maben, J. R.; Zetwo, M. P.; Springer-Young, M.; Galloway, J. N. *Geophys. Res. Lett.* **1993**, *20*, 699.
(4) Keene, W. C.; Sander, R.; Pszenny, A. A. P.; Vogt, R.; Crutzen, P. J.; Galloway, J. N. *J. Aerosol Sci.* **1998**, *29*, 339.
(5) Jacob, D. J. *Atmos. Environ.* **2000**, *34*, 2131.
(6) Gard, E. E.; Kleeman, M. J.; Gross, D. S.; Hughes, L. S.; Allen, J. O.; Morrical, B. D.; Fergenson, D. P.; Dienes, T., Galli, M. E.; Johnson, R. J.; Cass, G. R.; Prather, K. A. *Science* **1998**, *279*, 1184.
(7) Hughes, L. S.; Allen, J. O.; Bhave, P.; Kleeman, M. J.; Cass, G. R.; Liu, D.-Y.; Fergenson, P.; Morrical, B. D.; Prather, K. A. *Environ. Sci. Technol.* **2000**, *34*, 3058.
(8) Finlayson-Pitts, B. J.; Hemminger, J. C. *J. Phys. Chem. A* **2000**, *104*, 11463.
(9) Keene, W. C.; Maben, J. R.; Pszenny, A. A. P.; Galloway, J. N. *Environ. Sci. Technol.* **1993**, *27*, 866.
(10) Spicer, C. W.; Chapman, E. G.; Finlayson-Pitts, B. J.; Plasteridge, R. A.; Hubbe, J. M.; Fast, J. D.; Berkowitz, C. M. *Nature* **1998**, *394*, 353.
(11) Khalil, M. A. K.; Moore, R. M.; Harper, D. B.; Lobert, J. M.; Erickson, D. J.; Koropalov, V.; Sturges, W. T.; Keene, W. C. *J. Geophys. Res.* **1999**, *104*, 8333.
(12) Erickson, D. J.; Seuzaret, C.; Keene, W. C.; Gong, S. L. *J. Geophys. Res.* **1999**, *104*, 8347.
(13) Keene, W. C.; Khalil, M. A. K.; Erickson, D. J.; McCulloch, A.; Graedel, T. E.; Lobert, J. M.; Aucott, M. L.; Gong, S. L.; Harper, D. B.; Kleiman, G.; Midgley, P.; Moore, R. M.; Seuzaret, C.; Sturges, W. T.; Berkowitz, C. M.; Koropalov, V.; Barrie, L. A.; Li, Y. F. *J. Geophys. Res.* **1999**, *104*, 8429.
(14) Gong, S. L.; Barrie, L. A.; Prospero, J. M.; Savoie, D. L.; Ayers, G. P.; Blanchet, J.-P.; Spacek, L. *J. Geophys. Res.* **1997**, *102*, 3819.
(15) Reynolds, S. Utah Division of Air Quality Planning Brach, State of Utah, http://www.deq.state.ut.us/EQAIR/PLANNING/Chlorine.htm (accessed Jan 2002).
(16) Harris County, Texas, Pollution Control Division, Harris County Public Health & Environmental Services, http://www.hd.co.harris.tx.us/pcd/ (accessed Jan 2002).
(17) California Energy Commission, State of California, http://www.energy.ca.gov/database/index.html#powerplants (accessed Jan 2002).
(18) McRae, G. J.; Goodin, W. R.; Seinfeld, J. H. *Atmos. Environ.* **1982**, *16*, 679.
(19) McRae, G. J.; Seinfeld, J. H. *Atmos. Environ.* **1983**, *17*, 501.
(20) Harley, R. A.; Russell, A. G.; McRae, G. J.; Cass, G. R.; Seinfeld, J. H. *Environ. Sci. Technol.* **1993**, *27*, 378.
(21) Meng, Z.; Dabdub, D.; Seinfeld, J. H. *Science* **1997**, *277*, 166.
(22) Meng, Z.; Dabdub, D.; Seinfeld, J. H. *J. Geophys. Res.* **1998**, *103*, 3419.
(23) Griffin, R. J.; Dabdub, D.; Kleeman, M. J.; Fraser, M. P.; Cass, G. R.; Seinfeld, J. H. *J. Geophys. Res.* **2002**, 107.
(24) Griffin, R. J.; Dabdub, D.; Seinfeld, J. H. *J. Geophys. Res.* **2002**, 107.
(25) Kim, Y. P.; Seinfeld, J. H.; Saxena, P. *Aerosol Sci. Technol.* **1993**, *19*, 157.
(26) Meng, Z.; Seinfeld, J. H.; P. Saxena, P.; Kim, Y. P. *Aerosol Sci. Technol.* **1995**, *23*, 131.
(27) Pun, B. K.; Griffin, R. J.; Seigneur, C.; Seinfeld, J. H. *J. Geophys. Res.* **2002**, *107*.
(28) Woolf, D. K.; Bowyer, P. A.; Monahan, E. C. *J. Geophys. Res.* **1987**, *92*, 5142.
(29) Fitzgerald, J. W. *Atmos. Chem.* **1991**, *25A*, 533.
(30) Spiel, D. E. *J. Geophys. Res.* **1995**, *100*, 4995.
(31) Spiel, D. E. *J. Geophys. Res.* **1998**, *103*, 24907.
(32) Andreas, E. L. *J. Phys. Oceanogr.* **1998**, *28*, 2175.
(33) Andreas, E. L.; Edson, J. B.; Monahan, E. C.; Rouault, M. P.; Smith, S. T. *Boundary-Layer Meteorol.* **1995**, *72*, 3.
(34) Andreas, E. L.; Pattison, M. J.; Belcher, S. E *J. Geophys. Res.* **2001**, *106*, 7157.
(35) O′Dowd, C. D.; Smith, M. H. *J. Geophys. Res.* **1993**, *98*, 1137.
(36) Smith, M. H.; Park, P. M.; Consterdine, I. E. *Q. J. R. Meterol. Soc.* **1993**, *119*, 809.
(37) Stramska, M.; Marks, R.; Monahan, E. C. *J. Geophys. Res.* **1990**, *95*, 18281.
(38) Monahan, E. C.; Spiel, D. E.; Davidson, K. L. In *Oceanic Whitecaps*; Monaham, E. C., Mac Niocaill, G., Eds.; D. Riedel: Norwell, MA, 1986; pp 167−174.

(39) Gong, S. L.; Barrie, L. A.; Blanchet, J.-P. *J. Geophys. Res.* **1997**, *102*, 3805.
(40) De Leeuw, G.; Neele, F. P.; Hill, M.; Smith, M. H.; Vignati, E. *J. Geophys. Res.* **2000**, *105*, 29397.
(41) Vignati, E.; De Leeuw, G.; Berkowitz, R. *J. Geophys. Res.* **2001**, *106*, 20225.
(42) Atkinson, R.; Baulch, D. L.; Cox, R. A.; Hampson, R. F., Jr.; Kerr, J. A.; Rossi, M. J.; Troe, J. *J. Phys. Chem. Ref. Data* **1999**, *28*, 191.
(43) Atkinson, R.; Baulch, D. L.; Cox, R. A.; Hampson, R. F., Jr.; Kerr, J. A.; Rossi, M. J.; Troe, J. *J. Phys. Chem. Ref. Data* **2000**, *29*, 167.
(44) DeMore, W. B.; Sander, S. P.; Golden, D. M.; Hampson, R. F.; Kurylo, M. J.; Howard, C. J.; Ravishankara, A. R.; Kolb, C. E.; Molina, M. J. *Chemical Kinetics and Photochemical Data for Use in Stratospheric Modeling*: Report 97-4; Jet Propulsion Laboratory: Pasadena, CA, 1997.
(45) Sander, S. P.; Friedl, R. R.; DeMore, W. B.; Golden, D. M.; Kurylo, M. J.; Hampson, R. F.; Huie, R. E.; Moortgat, G. K.; Ravishankara, A. R.; Kolb, C. E.; Molina, M. J. *Chemical Kinetics and Photochemical Data for Use in Stratospheric Modeling*; Report 00-3; Jet Propulsion Laboratory: Pasadena, CA, 2000.
(46) Atkinson, R. *J. Phys. Chem. Ref. Data* **1997**, *26*, 215.
(47) Pilgrim, J. S.; McIlroy, A.; Taatjes, C. A. *J. Phys. Chem. A* **1997**, *101*, 1873.
(48) Stutz, J.; Ezell, M. J.; Ezell, A. A.; Finlayson-Pitts, B. J. *J. Phys. Chem. A* **1998**, *102*, 8510.
(49) Coquet, S.; Ariya, P. *Int. J. Chem. Kinet.* **2000**, *32*, 478.
(50) Notario, A.; Mellouki, A.; Le Bras, G. *Int. J. Chem. Kinet.* **2000**, *32*, 62.
(51) Notario, A.; Mellouki, A.; Le Bras, G. *Int. J. Chem. Kinet.* **2000**, *32*, 105.
(52) Ragains, M. L.; Finlayson-Pitts, B. J. *J. Phys. Chem. A* **1997**, *101*, 1509.
(53) Finlayson-Pitts, B. J.; Keoshian, C. J.; Buehler, B.; Ezell, A. A. *Int. J. Chem. Kinet.* **1999**, *31*, 491.
(54) Ravishankara, A. R. *Science* **1997**, *276*, 1058.
(55) Knipping, E. M.; Lakin, M. J.; Foster, K. L.; Jungwirth, P.; Tobias, D. J.; Gerber, R. B.; Dabdub, D.; Finlayson-Pitts, B. J. *Science* **2000**, *288*, 301.
(56) Sander, R.; Crutzen, P. J. *J. Geophys. Res.* **1996**, *101*, 9121.
(57) Vogt, R.; Crutzen, P. J.; Sander, R. *Nature* **1996**, *383*, 327.
(58) Hermann, H.; Ervens, B.; Jacobi, H.-W.; Wolke, R.; Nowacki, P.; Zellner, R. *J. Atmos. Chem.* **2000**, *36*, 231.
(59) Moldanova, J.; Ljungstrom, E. *J. Geophys. Res.* **2001**, *106*, 1271.
(60) Toyota, K.; Takahashi, M.; Akimoto, H. *Geophys. Res. Lett.* **2001**, *28*, 2899.
(61) Oum, K. W.; Lakin, M. J.; DeHaan, D. O.; Brauers, T.; Finlayson-Pitts, B. J. *Science* **1998**, *279*, 74.
(62) Knipping, E. M.; Dabdub, D. *J. Geophys. Res.* **2002**, 107.
(63) Fenter, F. F.; Caloz, F.; Rossi, M. J. *J. Phys. Chem.* **1996**, *100*, 1008.
(64) Behnke, W.; George, C.; Scheer, V.; Zetzsch, C. *J. Geophys. Res.* **1997**, *102*, 3795.
(65) Schweitzer, F.; Mirabel, P.; George C. *J. Phys. Chem. A* **1998**, *102*, 3942.
(66) Gebel, M. E.; Finlayson-Pitts, B. J. *J. Phys. Chem. A* **2001**, *105*, 5178.
(67) Caloz, F.; Fenter, F. F.; Rossi, M. J. *J. Phys. Chem.* **1996**, *100*, 7494.
(68) Wincel, H.; Mereand, E.; Castleman, A. W. *J. Phys. Chem. A* **1997**, *101*, 8248.
(69) Schwartz, S. E. In *Chemistry of Multiphase Atmospheric Systems*; NATO ASI Series; Jaeschke, W., Ed.; Springer-Verlag: Berlin, 1986; Vol. G6.
(70) Behnke, W.; Scheer V.; Zetzsch, C. *J. Aerosol Sci.* **1994**, *25*, S277−S278.
(71) Hanson, D. R. *J. Phys. Chem. B* **1997**, *101*, 4998.
(72) Hanson, D. R.; Ravishankara, A. R.; Solomon, S. *J. Geophys. Res.* **1994**, *99*, 3615.
(73) Donaldson, D. J.; Ravishankara, A. R.; Hanson, D. R. *J. Phys. Chem. A* **1997**, *101*, 4717.
(74) Robinson, G. N.; Worsnop, D. R.; Jayne, J. T.; Kolb, C. E.; Davidovits, P. *J. Geophys. Res.* **1997**, *102*, 3583.
(75) International Union of Pure and Applied Chemistry, Subcommittee for Gas Kinetic Data Evaluation, http://www.iupac-kinetic.ch.cam.ac.uk/r_het.php (accessed Jan 2002).
(76) Fraser, M. P.; Kleeman, M. J.; Schauer, J. J.; Cass, G. R. *Environ. Sci. Technol.* **2000**, *34*, 1302.
(77) Knipping, E. M.; Dabdub, D. *Atmos. Environ.* **2002**, *36*, 5741−5748.
(78) Fraser, M. P.; Grosjean, D.; Grosjean, E.; Rasmussen, R. A.; Cass, G. R. *Environ. Sci. Technol.* **1996**, *30*, 1731.
(79) Seinfeld, J. H.; Pandis, S. *Atmospheric Chemistry and Physics: From Air Pollution to Climate Change*; Wiley: New York, 1998.
(80) Rudich, Y.; Talukdar R. K.; Ravishankara, A. R. *J. Geophys. Res.* **1996**, *101*, 21023.
(81) Seisel, S.; Fluckiger, B.; Caloz, F.; Rossi, M. J. *Phys. Chem. Chem. Phys.* **1999**, *1*, 2257.
(82) Gershenzon, M. Y.; Ilin, S.; Fedotov, N. G.; Gershenzon, Y. M.; Aparina, E. V.; Zelenov, V. V. *J. Atmos. Chem.* **1999**, *34*, 119.
(83) Sadanada, Y.; Hirokawa, J.; Akimoto, H. *Geophys. Res. Lett.* **2001**, *28*, 4433.
(84) Tanaka, P. L.; Oldfield, S.; Neece, J. D.; Mullins, C. B.; Allen, D. T. *Environ. Sci. Technol.* **2000**, *34*, 4470.
(85) Chang, S.; McDonald-Buller, E.; Kimura, Y.; Yarwood, G.; Neece, J.; Russell, M.; Tanaka, P.; Allen, D. *Atmos. Environ.* **2002**, *36*, 4991.
(86) Finlayson-Pitts, B. J.; Pitts, J. N., Jr. *Science* **1997**, *276*, 1045.
(87) Finlayson-Pitts, B. J.; Pitts, J. N., Jr. *Chemistry of the Upper and Lower Atmosphere: Theory, Experiments and Applications*; Academic Press: San Diego, 2000.

Received for review May 15, 2002. Revised manuscript received October 22, 2002. Accepted October 28, 2002.

ES025793Z